

PAPER • OPEN ACCESS

## A data-informed analytic model for turbine power prediction with anisotropic local blockage effects

To cite this article: Marcus C R Juniper and Takafumi Nishino 2022 *J. Phys.: Conf. Ser.* **2265** 022046

View the [article online](#) for updates and enhancements.

### You may also like

- [Investigation of the nacelle blockage effect for a downwind turbine](#)  
Benjamin Anderson, Emmanuel Branlard, Ganesh Vijayakumar et al.
- [Simulation study of turbulent mixing characteristics of tight lattice with triangular arrangement under blockage condition](#)  
Yunxiang Li, Dongmei Luo, Xinyu Yang et al.
- [Optimizing the throughput of particulate streams subject to blocking](#)  
G Page, J Resing, P Viot et al.



## ECS Membership = Connection

### ECS membership connects you to the electrochemical community:

- Facilitate your research and discovery through ECS meetings which convene scientists from around the world;
- Access professional support through your lifetime career;
- Open up mentorship opportunities across the stages of your career;
- Build relationships that nurture partnership, teamwork—and success!

Join ECS!

Visit [electrochem.org/join](https://electrochem.org/join)



# A data-informed analytic model for turbine power prediction with anisotropic local blockage effects

Marcus C R Juniper and Takafumi Nishino

Department of Engineering Science, University of Oxford, Parks Road, Oxford, OX1 3PJ

E-mail: [marcus.juniper@eng.ox.ac.uk](mailto:marcus.juniper@eng.ox.ac.uk)

**Abstract.** This paper presents a new analytic approach for estimating the local power coefficient of a turbine experiencing anisotropic local blockage effects. Data-driven methods are employed first to approximately obtain a known analytic expression for isotropic local blockage effects, and then deployed to find candidate expressions for anisotropic local blockage effects. The dataset for the analysis of anisotropic local blockage is collected from 3D Reynolds-averaged Navier-Stokes (RANS) simulations of an infinitely wide array of actuator disks for nearly 2,000 different blockage configurations. This study builds upon previous work in array optimisation of both tidal and wind turbines, where the local power coefficient may increase substantially for optimal array configuration. A brief discussion on the relationship between the local blockage and wind farm blockage is also provided. Other theoretical approaches and possible refinements to the presented analytic model are also discussed.

## 1. Introduction

Understanding the theoretical optimal efficiency of a turbine is crucial for maximising the total power of both wind and tidal farms. Many physical factors impact the theoretical optimal efficiency. For example, Garrett and Cummins [1] (GC07) showed analytically how the Lanchester-Betz-Joukowski limit could be exceeded by considering a turbine in a channel. However, contrary to the assumption in the GC07 model, wind turbines in a wind farm do not experience blockage equally, i.e., there is a difference between the blockage effects experienced in each direction, from the ground, its sides (due to neighbouring turbines), and above (due to an atmospheric capping layer). This anisotropic local blockage effect results in GC07 being inaccurate in its prediction of turbine performance, as discussed later in this paper. Although there are experiments and simulations exploring the impact of anisotropic blockage [2; 3], there is little theoretical work to accurately predict its impact on wind turbines in a wind farm. The aim of this study is to create a theoretical framework, informed by data, for predicting the impact of anisotropic local blockage effects.

## 2. RANS simulations

In this section we detail the 3D RANS simulations of an infinitely wide array of (non-rotational) actuator disks used to explore the impact of anisotropic local blockage effects. We first present the flow and turbine set-up followed by a description of the computational grid along with a mesh validation study.



### 2.1. Computational methods

The 3D incompressible RANS equations are solved, modelling the Reynolds stress terms using the standard  $k - \epsilon$  model of Launder and Spalding [4]. The computations are conducted using ANSYS FLUENT 2021 R2 and performed as steady state. This RANS actuator disk method has been utilised successfully in the past [3; 5]; in particular, it has been shown to agree well with the classical, 1D inviscid actuator disk theory when used with low levels of ambient turbulence. In this study we also see close agreement with the GC07 model for a turbine in the centre of a square domain for all blockage ratios.

The simulations are carried out with a uniform inflow profile with streamwise velocity of  $U_{in} = 10\text{m/s}$ . For the low level of ambient turbulence, we set the turbulent quantities as  $k = 0.00015\text{m}^2/\text{s}^2$  and  $\epsilon = 3.02 \times 10^{-7}\text{m}^2/\text{s}^3$  at the inlet. The air density and viscosity are held constant at  $1.225\text{kg/m}^3$  and  $1.78 \times 10^{-5}\text{kg/ms}$ , respectively. Although a turbine in a realistic environment may experience blockage effects from an atmospheric capping layer above, we do not consider the stratification or vertical shear of the inflow for simplicity. Symmetry conditions are applied to the top, bottom and side boundaries to mimic the configuration considered by the GC07 model, which represents (part of) an infinitely wide row of turbines.

### 2.2. Computational grid: mesh test

Figure 1 shows an example of a 2D slice of the computational mesh at the turbine plane. To make the 3D mesh this 2D slice is propagated in the streamwise direction (both upstream and downstream) to make a computational mesh consisting of exclusively hexahedral cells. The slices are spaced non-uniformly with minimum spacing of  $0.003D$ , where  $D = 100\text{m}$  is the disc diameter, nearest to the turbine plane. The mesh inside the  $0.75D \times 1.5D$  rectangle around the half turbine is held constant across all different blockage cases considered in this study. Different sized domains are defined by three values,  $H_B$ ,  $H_A$  and  $W$ , which are the hub height, distance from the hub to the top of the domain, and the domain width, respectively.  $H_A$  and  $H_B$  take 17 non-equidistant values between  $0.75D$  and  $20.5D$  and  $W$  takes 13 non-equidistant values between  $0.75D$  and  $10.5D$ . For convenience, the three parameters which dictate the size and configuration of the simulated domain will be written as the triple  $(H_B, H_A, W)$ . Not all combinations of values are considered as due to the symmetry of the system for example  $(0.75D, 10.5D, 2D) = (10.5D, 0.75D, 2D)$ , and the total height ( $H_B + H_A$ ) is limited to  $21.5D$ , resulting in 1989 different domains simulated for this study.

A grid sensitivity study was conducted for the domain sized  $(0.75D, 0.75D, 0.75D)$ . The lower resolution grid had a total of 157200 cells and was compared against a fine resolution grid of 1063200 cells. The domain was chosen as the high shear present in these simulations would be sensitive to grid resolution. We define a 'local' or 'internal' power coefficient  $C_p^*$  as

$$C_p^* = \frac{P}{\frac{1}{2}\rho U_{in}^3 A} \quad (1)$$

where  $P$  is the power of the turbine,  $A$  is the turbine swept area, and  $\rho$  the fluid density. As can be seen in figure 2 the two cases are near identical for all values of the disc resistance coefficient  $K$ , with a difference in  $C_p^*$  of less than 0.1% for all  $K$  values tested, suggesting that the lower resolution mesh is sufficient for this study.

## 3. Wind-farm blockage vs local blockage

In this section we will clarify what is meant by the 'internal' performance increases due to local blockage effects; this is not to be confused with wind-farm blockage effects [6] which reduce the power of a wind farm as a portion of the incoming flow bypasses the entire farm.

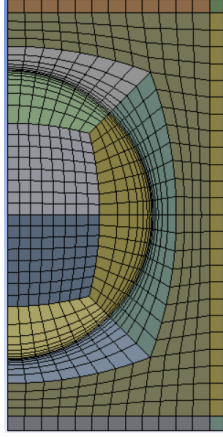


**Figure 1.** Cross-sectional segment of the computational mesh around the actuator half-disk at lower resolution.

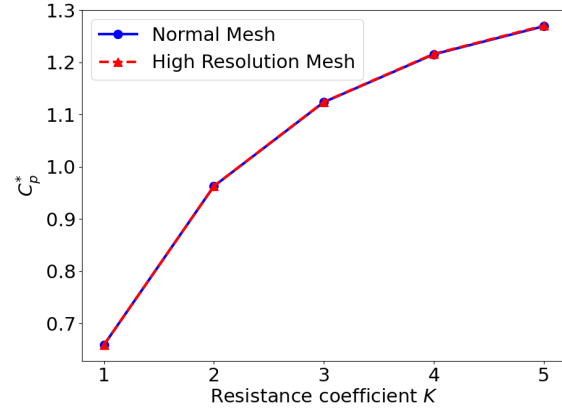


**Figure 2.** Impact of grid resolution on  $C_p^*$  for the highest blockage case.

Firstly, we must set out how we define the power coefficient of a turbine. Alongside the local power coefficient  $C_p^*$ , we also define the 'global' power coefficient  $C_p$

$$C_p = \frac{P}{\frac{1}{2}\rho U_0^3 A} \quad (2)$$

where  $U_0$  is undisturbed or 'natural' wind speed observed when the whole wind farm does not exist. Therefore,  $C_p$  is a measure of 'overall' efficiency including the power loss due to the wind-farm blockage. The local power coefficient  $C_p^*$  is a measure of 'internal' efficiency, which does not include the power loss due to the wind farm blockage.

To illustrate the impact of local blockage on the overall and internal efficiencies, we will compare how the global power coefficient  $C_p$  and the local power coefficient  $C_p^*$  change as we alter the lateral turbine spacing in the infinitely wide row of turbines. For this exploration we keep hub height ( $H_B$ ) and the height of the domain ( $H_A + H_B$ ) fixed at  $0.75D$  and  $21.25D$  respectively.

We calculate  $C_p^*$  directly from the RANS simulations, whereas  $C_p$  is estimated by combining the RANS results with the two-scale momentum theory approach of Nishino and Dunstan [7] (for full details see the original paper). Here  $C_p = \beta^3 C_p^*$  where  $\beta = U_{in}/U_0$ . To estimate this unknown velocity ratio from the theory, we consider that there are multiple rows of turbines placed equidistantly with a large streamwise spacing of  $20D$ , and assume that this distance is large enough for each turbine wake to be fully recovered. This allows us to calculate the array density  $\lambda$  and the local thrust coefficient  $C_T^*$  to be used in the theory, which eventually gives  $\beta$  as a function of an external (mesoscale) flow parameter  $\zeta$ . Here  $\zeta$  is the momentum response parameter for the atmosphere, which represents the ability of the atmosphere to sustain wind speeds against the resistance caused by the wind farm. Typical values of which are expected to be between 5 and 25 for a realistic offshore wind farm [8]. As shown in figure 3 as we decrease the lateral turbine spacing the global power coefficient  $C_p$  falls for all values of  $\zeta$  between 5 and 25. However, the local power coefficient  $C_p^*$  increases as we decrease the lateral spacing. It is the local power coefficient that we concern ourselves with in this study and how to improve upon current analytical techniques to estimate  $C_p^*$  for turbines which experience local blockage anisotropically.

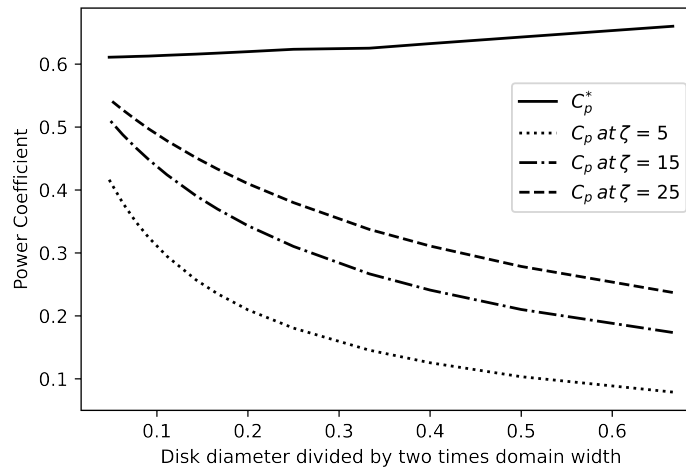


**Figure 3.** Local and global power coefficients plotted against the lateral blockage ratio ( $D/2W$ ).

Complexity	MSE	Equation
1	2.46749	1.847
2	1.69148	$\exp^B$
3	0.15287	$5.712 * B$
4	0.13487	$10.4 * B^2$
5	0.01157	$\frac{1}{(1.13-B)^2}$
6	0.00188	$\frac{1}{1.69*(1-B)}$
7	0.00003	$\frac{0.589}{(1-0.986*B)^2}$

**Table 1.** Suggested analytical functions for the isotropic blockage effect on  $C_{p\max}^*$  found by symbolic regression along with their complexity and mean-squared error (MSE).

## 4. RANS simulation results

### 4.1. Symbolic regression for isotropic local blockage

Before presenting the results of 3D RANS simulations, we first present 2D RANS results, analysed using symbolic regression to showcase the technique for wind energy. The regression is run using an open source code called PySr [9]. The motivation is that many physical systems can be accurately modelled with relatively concise analytic expressions. Symbolic regression works by testing some set of given functions against the data and rewarding functions which best fit the data. An actuator disk (or line segment in the 2D system) of diameter 100m was placed in the middle of a 2D rectangular channel with 19 different heights to simulate a range of blockage ratios,  $B$ , from 2% to 66%. Where  $B = A_t/A_{total}$  where  $A_t$  is the area of the turbine and  $A_{total}$  is the height of the domain. The other conditions remain identical to those detailed for the 3D RANS simulations. The symbolic regression method applied to the 2D RANS results suggested  $C_{p\max}^* = \frac{0.589}{(1-0.986*B)^2}$  for the analytical function to describe the isotropic blockage effect. This is promising as not only does it find the format of the function it also closely approximates the true analytical equation  $C_{p\max}^* = \frac{16}{27(1-B)^2}$ . The raw 2D RANS data differed from the analytical solution by as much as 3.5%, so although more accurate data is beneficial the method can find promising results on relatively few and non-exact data points. The algorithm was fed many

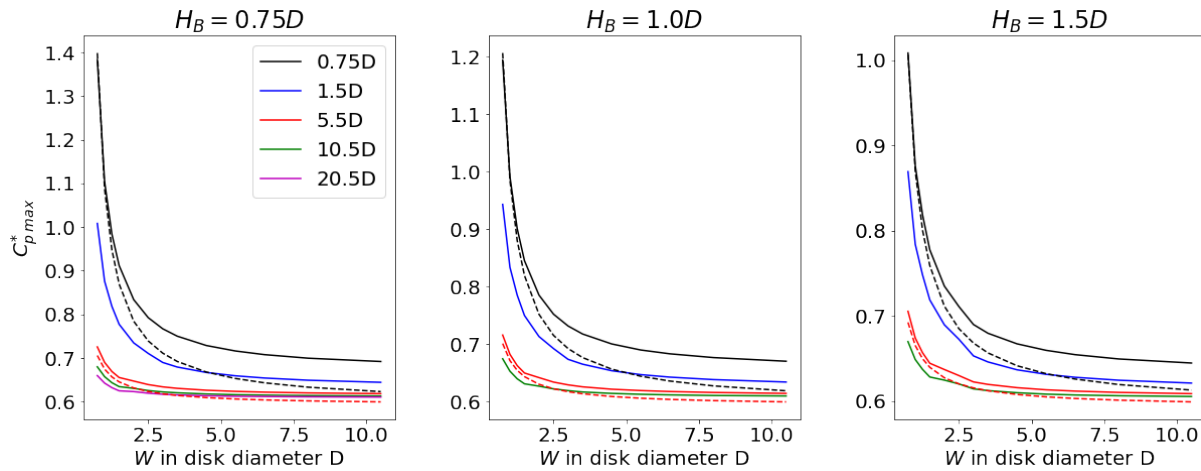


**Figure 4.** Effects of anisotropic local blockage on  $C_{pmax}^*$ . Solid lines are 3D RANS results. Dashed lines are GC07 prediction based on isotropic blockage. Different colours represent different values of  $H_A$ .

test functions to ensure that the result is not a product of guiding the algorithm to the known solution. A list of 7 equations, of varying complexity, suggested by the symbolic regression method are summarised in table 1.

#### 4.2. Anisotropic local blockage

A selection of the results from the 3D simulations are presented in figure 4. The maximum  $C_p^*$  values predicted from the GC07 model are also plotted for comparison. We can observe that GC07 consistently under-predicts the power coefficient in an anisotropically blocked domain. This is understandable as GC07 assumes that the turbine is at the centre of the domain. Although a large number of simulations were conducted for this particular study these simulations require a decent amount of computational resources; therefore it would be desirable if anisotropic local blockage effect could also be predicted through computationally faster analytical models.

### 5. New method

The creation of a new method to estimate  $C_p^*$  for a turbine with an anisotropic local blockage has been attempted using data-driven methods. First, a series of refined analytical equations were obtained for the 3D problem from symbolic regression. The analytic equations obtained from this exploration improved on GC07 but they appeared as over fitted equations with large exponents rather than concise equations describing interpretable physics. Hence, in this section we will aim to create a new method in a different manner.

The inspiration for this new method is rooted in the two-scale actuator disk model set out by Nishino and Willden [10]. Although this two-scale model was originally proposed for a short array of tidal turbines with isotropic local blockages, Nishino and Draper [3] found that the model could be applied to this anisotropic case as well, where 3D RANS predicts  $C_{pmax} = 0.65$  (for domain,  $H_B = 1D$ ,  $W = 0.75D$  and  $H_A = 24D$ ) and the two-scale model predicts  $C_{pmax} = 0.71$ . The method presented below improves upon that with a prediction of  $C_{pmax} = 0.66$ .

The basic assumption made here for the new method is that the system can be approximately described using linear momentum actuator disk theory (LMADT) [11] by decomposing the expansion of flow through the disk into three distinct but coupled sub-expansion processes.

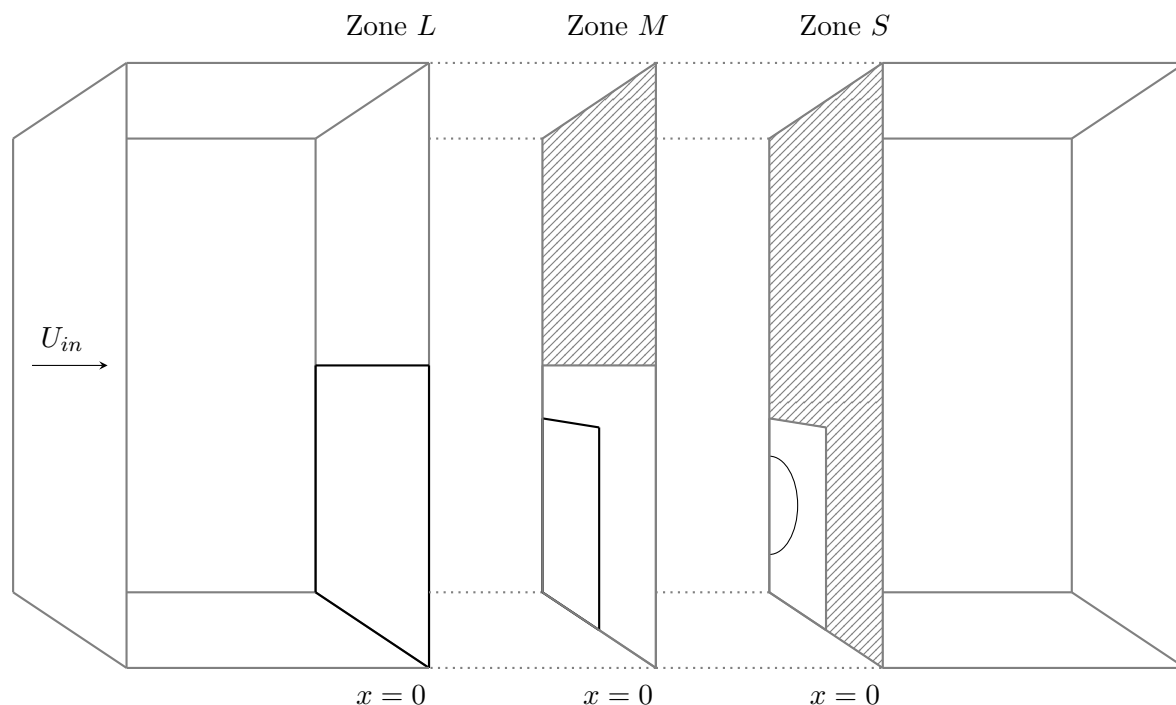


**Figure 5.** Schematic of the new method. Each black outlined shape is an actuator disk/surface, the grey lined zones are ignored when we focus on the actuator disk/surface in that domain.

The new method begins by considering three sub-domains alongside the actuator disk. One is around the turbine itself, defined as the smallest box centred on the turbine which has an edge meeting a boundary (see figure 5); we will refer to this box as the small sub-domain, zone  $S$ . The middle sub-domain is defined as the smallest box centred on the turbine which meets at least one additional boundary than the small sub-domain, zone  $M$ . The largest sub-domain is defined as the next smallest box that meets an additional boundary to the middle sub-domain and consequently will always be the whole cross-sectional domain, zone  $L$ .

The turbine, smallest and middle sub-domains are treated as actuator surfaces at the turbine plane with distinct blockage ratios and resistance coefficients. The smallest sub-domain has total area  $A_s$ , middle  $A_m$  and largest  $A_l$ . The subscripts  $t, s, m, l$  will hereafter refer to the turbine, smallest sub-domain, middle sub-domain and largest sub-domain respectively. Blockage ratios between these three created domains and the size of the turbine  $A_t$  may be defined as  $B_s = A_t/A_s$ ,  $B_m = A_s/A_m$  and  $B_l = A_m/A_l$ .

We first assume the actuator surface being considered is contained within a uniform channel with the cross-sectional area that is equal to the maximum size of the streamtube passing through the sub-domain actuator that most immediately surrounds the considered surface (e.g. the small sub-domain when the considered surface is the turbine). This allows us to use the LMADT to calculate the expansion of flow through the considered surface. However, the true region in which the considered disk/surface operates in is not uniform as assumed in the LMADT. This problem is overcome in this new method by introducing a key assumption that the proportion of upstream flow that passes through the turbine remains constant between the 'uniform' and 'true' cases.

To illustrate the above assumptions we discuss a simplified 2D system containing only two actuator surfaces instead of three, i.e., the turbine and the small sub-domain actuators, as depicted in figure 6. The LMADT equations are solved for the small sub-domain as an actuator

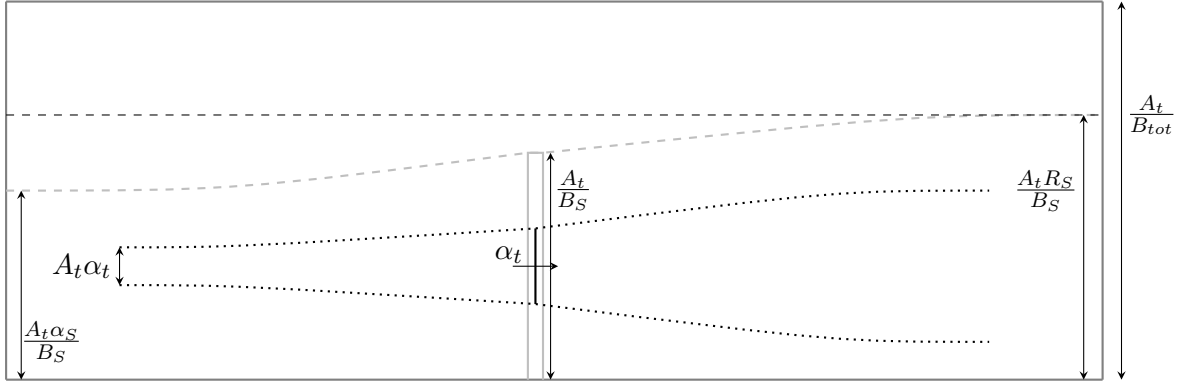


**Figure 6.** Schematic of the '2D' case for illustration of 'uniform' and 'true' flow passages. The solid black line is the turbine, the grey box encompassing it is the small sub-domain actuator, the grey dashed line is the 'true' bounding region, the black dashed line is the 'uniform' bounding region.

disk in a domain sized  $A_t/B_{tot}$  with resistance coefficient  $K_s$ . The streamtube which passes through the small sub-domain actuator starts with size  $\alpha_s A_t/B_s$  in the upstream, flows through the surface of area  $A_t/B_s$  with speed  $\alpha_s U_{in}$ , and then expands to the size of  $R_s A_t/B_s$  in the downstream position. The blockage ratio for the turbine (for the hypothetical 'uniform' case) is now set as the ratio of the turbine area,  $A_t$ , to the largest size of the streamtube which bounds it,  $R_s A_t/B_s$ . Then applying the LMADT to the turbine with resistance coefficient  $K_t$ , a flow speed through the turbine (non-dimensionalised by the inflow speed  $U_{in}$ )  $\alpha_t$  is obtained. This means that in this hypothetical 'uniform' case, the proportion  $\alpha_t$  of the inflow passes through the turbine. By assuming that the same proportion of the upstream flow passes through the turbine area in the 'true' case, we eventually obtain  $A_t \alpha_t \alpha_s / R_s$  as the true upstream domain width (instead of  $A_t \alpha_t$ ) for the streamtube passing through the turbine area. Therefore, through conservation of mass, the true flow speed through the turbine (non-dimensionalised by  $U_{in}$ ) is obtained as  $\alpha_t \alpha_s / R_s$  instead of  $\alpha_t$ .

The final step to construct this model is describing a relationship between the resistance coefficients for each actuator surface given a resistance coefficient for the turbine  $K_t$ . For the simplified 2D case discussed above, the relationship we adopt is described as

$$K_s = K_t \alpha_t^2 \alpha_s \frac{B_s}{R_s^4} \quad (3)$$

Using the relation of  $K$  to the thrust  $T$  from LMADT, i.e.,  $T = \frac{1}{2} \rho A K (\alpha u)^2$ , again with appropriate subscripts, and  $\rho$  the density of the fluid, (3) can be rewritten as:

$$T_s = T_t \frac{\alpha_s}{R_s^2} \quad (4)$$

This is equivalent to saying, the thrust of the small sub-domain actuator ( $T_s$ ) scaled to the size of the downstream recovery ( $R_s$ ) is equal to the thrust of the turbine ( $T_t$ ) scaled by the expansion rate of the streamtube passing through the small sub-domain ( $\alpha_s/R_s$ ). By applying the same approach to the original 3D system (containing three actuator surfaces instead of two), we have now obtained all three resistance coefficients and three blockage ratios for all three sub-domains. Finally we numerically solve the LMADT equations for these three coupled sub-domains and calculate the value of  $C_p^*$  as

$$C_p^* = K_t \left( \frac{\alpha_t \alpha_s \alpha_m}{R_s R_m} \right)^3 \quad (5)$$



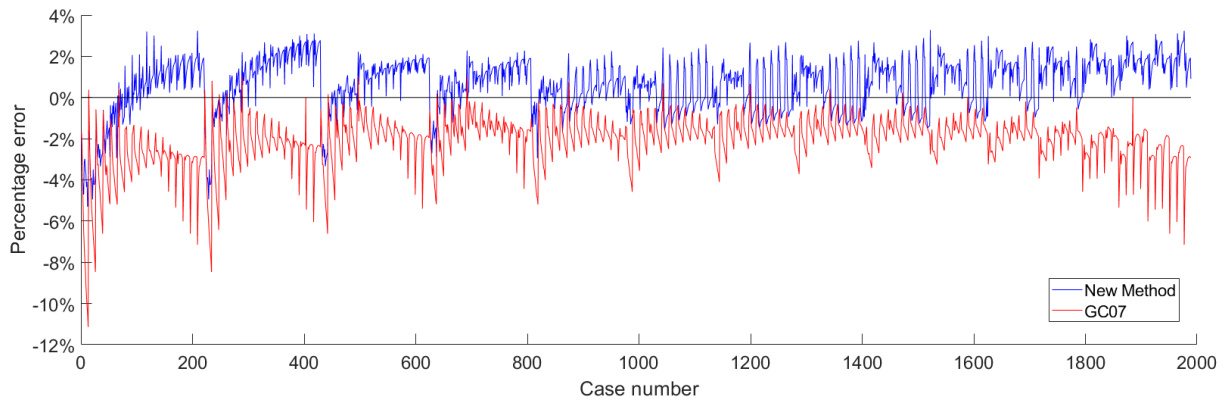


**Figure 7.** Percentage error of  $C_p^*$  between the two analytical predictions and RANS data.

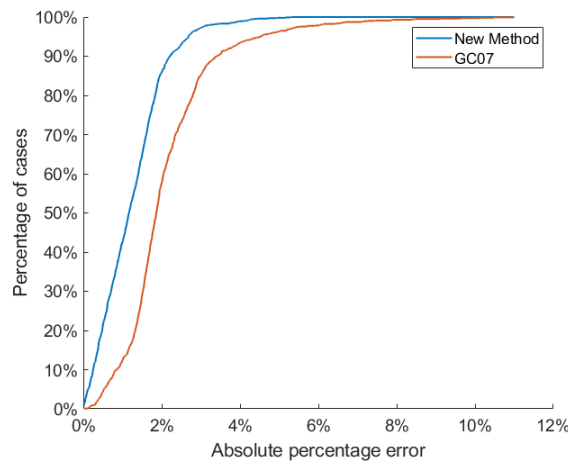


**Figure 8.** Cumulative distribution function for the absolute percentage error of  $C_p^*$  between the two analytic methods and the RANS simulation data.

This method has the advantage of very low computational costs, taking about 0.1s to make a prediction (for a given blockage configuration) running on a single core, compared to the RANS simulations which can take several minutes to make a prediction when running on multiple cores.

### 5.1. Validation

The percentage error, defined as one minus the power coefficient obtained from data (3D RANS) divided by the predicted coefficient ( $1 - C_{p,Data}^*/C_{p,Pred}^*$ ), is plotted for both methods in figure 7, where the x-axis is the case number. The new method not only reduces the absolute mean error from 2.1% of GC07 down to 1.2% it also reduces the maximum error from 11% to 5%. It should be noted that the relationship between the thrust at each sub-domain (given in eq. (4) for the 2D case) has been given arbitrarily in this model (based partly on physical intuition but also on the close agreement of the outcome with the RANS data; in this sense, the model may be referred to as a 'data-informed' analytic model). Hence, it is possible to further improve the agreement with the data by tuning the thrust relationship, although this is outside the scope of this paper.

The cumulative distribution function for the absolute error in the new method and GC07 is

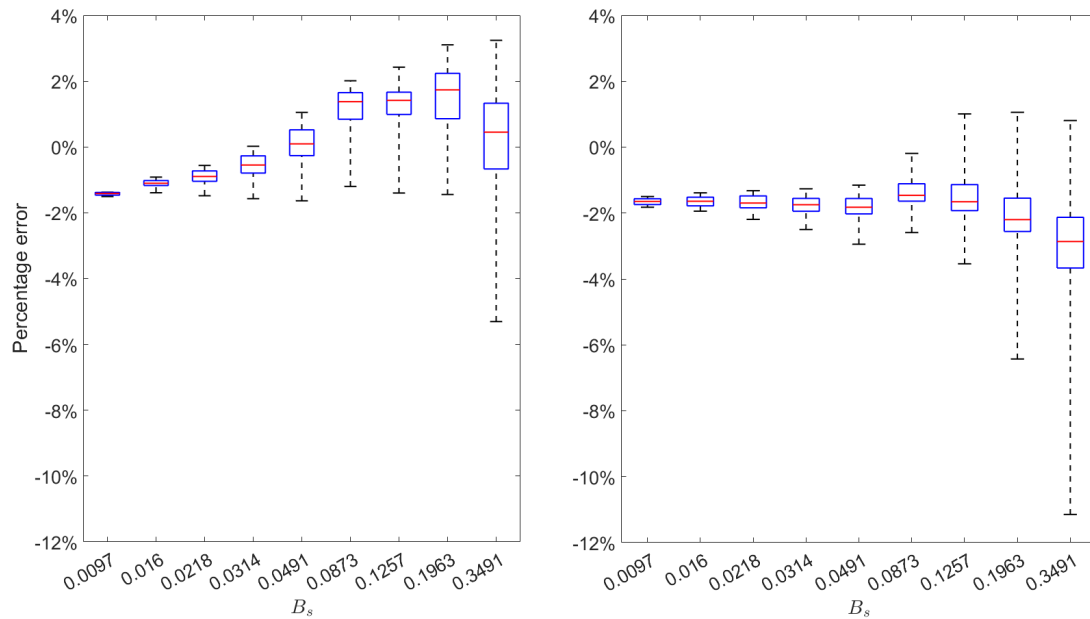


**Figure 9.** Percentage error of  $C_p^*$  with data for the new method (left) and GC07 (right) at various  $B_s$  values.

presented in figure 8. From this analysis we can observe that 50% of the new method predictions have up to a 1% error when compared to RANS data, whereas 50% of GC07 predictions have up to a 1.9% error. The new method however has up to 85% of its predictions existing within that same 1.9% error range, compared to the GC07 predictions where 85% of cases have up to a 3% error. Figure 9 shows the percentage error for the new method and GC07 predictions at various values of  $B_s$ . For each box the central mark indicates the median, and the bottom and top edges of the box indicate the 25th and 75th percentiles, respectively. The whiskers extend to the most extreme data points. Across all values of  $B_s$  the new method closely matched or improves upon GC07, suggesting the gains noted previously are across the whole parameter space. For low values of  $B_s$  both methods tend to give similar predictions, which is understandable as anisotropic local blockage effects diminish when  $B_s \rightarrow 0$ . However, even at the lowest  $B_s$  tested, the new method maintains a slightly increased precision. The new method maintains a better precision at higher values of  $B_s$ , where there are more cases in which anisotropic local blockage effects have a significant impact; with the range of error for the presented method as almost half that of GC07.

## 6. Discussion and conclusion

In this paper we have presented a series of studies on the calculation of  $C_p^*$  for turbines experiencing anisotropic local blockage effects. In section 3 the difference between the local blockage and wind-farm blockage effects were explored. We showed that although the global power coefficient drops due to wind-farm blockage, the local power coefficient rises as the lateral turbine spacing is reduced. Section 4.1 presented the utility of data-driven methods in their ability to obtain a physically interpretable analytic expression from data for isotropic local blockage effects. Although no concise single expression was obtained for the anisotropic local blockage effect, the ability of this method to extract a physical expression from data is clear and may be utilised for other explorations of data.

The new analytic model presented in section 5 shows clear improvement over the predictions made by the GC07 model and also provides a framework for new variants of data-informed models for anisotropic local blockage effects. Further advancements to the LMADT approach by including non-uniform inflows like those presented in [12] or considering the atmospheric capping layer as a free surface [13; 14], would allow an extension of the proposed model to make computationally fast power coefficient predictions for more realistic wind farm conditions.

A further study on the validity of the assumptions made in section 5 for the creation of this model should be conducted in the future to better understand the underlying physics of the system, although it should be remembered that this is not a purely theoretical model but a data-informed model (and hence the assumptions are partly justified by the good agreement with the data). It should also be noted that the RANS simulations presented and the use of LMADT are for low levels of free stream turbulence. Further investigations would be required to include the combined effects of turbulence and local blockage, such as those discussed in [5], into an analytical model.

### Acknowledgments

The authors gratefully acknowledge the support of the University of Oxford Advanced Research Computing (ARC) facility.

### References

- [1] Garrett C and Cummins P The efficiency of a turbine in a tidal channel 2007 *J. Fluid Mech.* **588** 243-51
- [2] Ross H and Polagye B An experimental evaluation of blockage effects on the wake of a cross-flow current turbine 2020 *J. Ocean Eng. Mar. Energy* **6** 263-75
- [3] Nishino T and Draper S Local blockage effect for wind turbines 2015 *J. Phys.:Conf. Ser.* **625** 012010
- [4] Launder B E and Spalding D B The numerical computation of turbulent flows 1974 *Comput. Methods Appl. Mech. Eng.* **3** 269-89
- [5] Nishino T and Willden R H J Effects of 3-D channel blockage and turbulent wake mixing on the limit of power extraction by tidal turbines 2012 *Int J. Heat Fluid Flow* **37** 123-35
- [6] Bleeg J, Purcell M, Ruisi R and Traiger E Wind Farm Blockage and the Consequences of Neglecting Its Impact on Energy Production 2018 *Energies* **11** 1609
- [7] Nishino T and Dunstan T D Two-scale momentum theory for time-dependent modelling of large wind farms 2020 *J. Fluid Mech.* **894** A2.
- [8] Patel K, Dunstan T D and Nishino T Time-Dependent Upper Limits to the Performance of Large Wind Farms Due to Mesoscale Atmospheric Response 2021 *Energies* **14** 6437
- [9] Cranmer M, Sanchez-Gonzalez A, Battaglia P, Xu R, Cranmer K, Spergel D and Ho S Discovering Symbolic Models from Deep Learning with Inductive Biases 2020 *Proc. NeurIPS*
- [10] Nishino T and Willden R H J Two-scale dynamics of flow past a partial cross-stream array of tidal turbines 2013 *J. Fluid Mech.* **730** 220-44
- [11] Juniper M C R and Nishino T Multi-row extension to laterally confined actuator disk model using a hybrid inviscid-viscous approach 2020 *Proc. 16th EAWC PhD Seminar* 33-40
- [12] Draper S, Nishino T, Adcock T and Taylor P H Performance of an ideal turbine in an inviscid shear flow 2016 *J. Fluid Mech.* **796** 86-112
- [13] Vogel C R, Housby G T and Willden R H J Effect of free surface deformation on the extractable power of a finite width turbine array 2016 *Renewable Energy* **88** 317-24
- [14] Housby G T, Draper S and Oldfield M L G Application of linear momentum actuator disc theory to open channel flow 2008 *Tech. Rep. OUEL 2296/08* University of Oxford